Atmospheric ammonia variability and link with particulate matter formation: a case study over the Paris area

Camille Viatte, Tianze Wang, Martin van Damme, Enrico Dammers, Frederik Meleux, Lieven Clarisse, Mark W. Shephard, Simon Whitburn, Pierre-François Coheur, Karen E. Cady-Pereira, et al.

Atmos. Chem. Phys. Discuss., https://doi.org/10.5194/acp-2019-138
Manuscript under review for journal Atmos. Chem. Phys.
Discussion started: 25 March 2019

Atmospheric Chemistry and Physics Discussions

Atmospheric ammonia variability and link with PM formation: a case study over the Paris area

Viatte Camille[1], Wang Tianze[1], Van Damme Martin[2], Dammers Enrico[3], Meleux Frederik[4], Clarisse Lieven[2], Shephard Mark W.[3], Whitburn Simon[2], Coheur Pierre François[2], Cady-Pereira Karen E.[5], and Clerbaux Cathy[1,2]

[1] LATMOS/IPSL, Sorbonne Université, UVSQ, CNRS, Paris, France
[2] Université libre de Bruxelles (ULB), Service de Chimie Quantique et Photophysique, Atmospheric Spectroscopy, Brussels, Belgium
[3] Environment and Climate Change Canada, Toronto, Ontario, Canada
[4] Institut national de l'environnement industriel et des risques, INERIS, Verneuil en Halatte, France
[5] Atmospheric and Environmental Research (AER), Inc., Lexington, USA

Atmos. Chem. Phys. Discuss., https://doi.org/10.5194/acp-2019-138
Manuscript under review for journal Atmos. Chem. Phys.
Discussion started: 25 March 2019

Atmospheric Chemistry and Physics Discussions

Abstract

The Paris megacity experiences frequent particulate matter ($PM_{2.5}$, PM with a diameter less than 2.5 µm) pollution episodes in springtime (March-April). At this time of the year, large parts of the particles consist of ammonium sulfate and nitrate which are formed from ammonia (NH_3) released during fertilizer spreading practices and transported from the surrounding areas to Paris. There is still limited knowledge on the emission sources around Paris, their magnitude and seasonality.

Using space-borne NH_3 observation records of 10-years (2008-2017) and 5-years (2013-2017) provided by the Infrared Atmospheric Sounding Interferometer (IASI) and the Cross-Track Infrared Sounder (CrIS) instrument, regional pattern of NH_3 variabilities (seasonal and inter-annual) are derived. Observations reveal identical high seasonal variabilities with three major NH_3 hot spots found from March to August. The high inter-annual variability is discussed with respect to atmospheric total precipitation and temperature.

A detailed analysis of the seasonal cycle is performed using both IASI and the CrIS instrument data, together with outputs from the CHIMERE atmospheric model. For months of high NH_3 concentrations (March to August) the CHIMERE model shows good correspondence with correlation slopes of 0.98 and 0.71 when comparing with IASI and CrIS, respectively. It is found that the model is only able to reproduce half of the observed atmospheric temporal NH_3 variability in the domain. In term of spatial variability, the CHIMERE monthly NH_3 concentrations in springtime show a slight underrepresentation over Belgium and the United-Kingdom and overrepresentation in agricultural areas in the French Brittany/Pays de la Loire and Plateau du Jura region, as well as in the north part of Switzerland.

Using HYSPLIT cluster analysis of back-trajectories, we show that NH_3 total columns measured in spring over Paris are enhanced when air masses are originated from the Northeast (e. g., Netherlands and Belgium), highlighting the long-range transport importance on the NH_3 budget over Paris.

Finally, we quantify the key meteorological parameters driving the specific conditions important for the $PM_{2.5}$ formation from NH_3 in the Ile-de-France region in springtime. Data-driven results based on surface $PM_{2.5}$ measurements from the Airparif network and IASI NH_3 observations show that a combination of the factors, e. g. a low boundary layer of ~500m, a relatively low temperature of 5°C and a high relative humidity of 70%, contributes to favor $PM_{2.5}$ and NH_3 correlation.

1. Introduction

Ammonia (NH_3) is an atmospheric pollutant and one of the main sources of reactive nitrogen in the atmosphere which is involved in numerous biochemical exchanges impacting all ecosystems [Sutton et al., 2013]. The global budget of reactive N has dramatically increased since the preindustrial era [Holland et al., 2005; Battye et al., 2017] causing major environmental damages such as ecosystems and species extinction, as well as soil and water eutrophication and acidification [Rockström et al., 2009]. NH_3 is a precursor of ammonium salts which can form up to 50% to particulate matter (PM) total mass [Behera et al., 2013]. Large cities such as Paris (which is the most populated area in the European Union with 10.5 million people when its larger metropolitan regions are included) typically experiences strong PM pollution episodes in springtime. These particles are known to be harmful for human health [Pope III et al., 2009] inducing 2000 deaths per year in the Paris megacity [Corso et al., 2016] and to impact the radiative budget of the Earth [Myhre et al., 2013].

Because of their impact on the environment, public health, and climate change, NH_3 emissions are regulated in several countries in the world. However, NH_3 emissions of European countries have increased by 2% over the period 2014-2016 [National Emission Ceilings Directive reporting status, 2018], where the Gothenburg Protocol set a reduction of 6% by 2020. In France, where 94% of NH_3 emissions come from the agriculture sector [CITEPA, 2018] as a result of extensive fertilizer use to increase crop yields [Erisman et al., 2008], policies have been implemented with the aim to reduce NH_3 emissions by 13% in 2030 related to 2005 [CEIP, 2016]. However NH_3 emissions are projected to increase in the future globally with increased population and food demand [van Vuuren et al., 2011] and NH_3 volatilization will be enhanced with climate change [Sutton et al., 2013].

Once in the atmosphere, NH_3 is rapidly removed by wet and dry deposition, and by reactions with atmospheric sulfuric and nitric acid, leading to a relatively short lifetime between a few hours and few days [Galloway et al., 2003]. Release of NH_3 in the atmosphere depends on i) agriculture practices: spreading season, fertilizer form (urea, ammonium nitrate), fertilizer application methods, crops, soil conditions such as pH [Hamaoui-Laguel et al., 2014]; and on ii) meteorological conditions (i.e. wind, temperature, and precipitation). Inter-annual variability of PM formation over urban area is poorly understood, since it also depends on many factors such as atmospheric humidity and temperature, which govern the phase equilibrium of secondary aerosols [Fuzzi et al., 2015]. The variety of factors influencing NH_3 volatilization and PM formation illustrates the complexity of predicting their concentrations in the atmosphere [Behera et al., 2013].

Atmospheric chemical transport models have difficulty representing both NH_3 and $PM_{2.5}$ distributions due to the challenge of reproducing NH_3 temporal variability [Pinder et al., 2006;

Fortems-Cheiney et al., 2016], long-range transport of pollutants [Moran et al., 2014], and secondary aerosol formation in the atmosphere [Petetin et al., 2016]. The GEOS-Chem chemical transport model [Bey et al., 2001] was found to underestimate the observed NH_3 concentrations in most regions of the globe [Zhu et al., 2013; Li et al., 2017]. Heald et al. (2012) compared the IASI observations with the GEOS-Chem model and showed that NH_3 is likely underestimated in California, leading to a local underestimate of ammonium nitrate aerosol. Similarly, the French CHIMERE model [Menut et al., 2013] underestimates the NH_3 budget over Paris [Petetin et al., 2016; Fortems-Cheiney et al., 2016] because of the mis-representation of agricultural emissions in terms of intensity and both spatial and temporal distribution. Often ground and aircraft-based observations are used to provide detailed representation of the atmospheric state that can be used to evaluate and improve the model simulations; however, these can be spatially sparse and/or over short sampling periods, especially globally. Additionally, more recently available (within the last 10-years) sun-synchronous satellite-based infrared sensors have been providing NH_3 observations globally with a spatial resolution of ~15 km approximately twice a day. These satellite observations have limited independent vertical information, but do capture the spatiotemporal variabilities needed to help address these issues and improve model simulations, especially in remote locations [Skjøth et al., 2011; Kranenburg et al., 2016].

Aside from the Tropospheric Emission Spectrometer (TES, [Beer et al., 2008]), now decommissioned but which was first to demonstrate the capability of thermal infrared instruments to monitoring lower tropospheric NH_3 , 3 missions are able to measure it now : the Atmospheric InfraRed Sounder (AIRS, [Warner et al., 2016]*)*, the Cross-track Infrared Sounder (CrIS, [Shephard and Cady-Pereira, 2015]), and the Infrared Atmospheric Sounding Interferometer (IASI, [Clarisse et al., 2009]). Recent studies have shown the increased capacity of space-borne instruments to derived spatial and seasonal distributions of NH_3 concentrations globally [Clarisse et al., 2009; Shephard et al., 2011; Van Damme et al., 2014a & 2015a], regionally [Beer et al., 2008; Clarisse et al., 2010; Van Damme et al., 2014b] and locally [Van Damme et al., 2018], as well as trends of NH_3 [Warner et al., 2017].

Representative measurements of NH_3 concentrations and spatiotemporal variabilities are needed to address the link between NH_3 and $PM_{2.5}$ formation and improve model simulations. This has been attempted previously in some cities around the world, such as in Shanghai [Ye et al., 2011], Houston [Gong et al., 2013], Santiago City [Toro et al., 2014], and Beijing [Zhao et al., 2016] for instance. However, although the Paris megacity is repeatedly shrouded by particulate pollution episodes, many of studies are limited and performed over relatively short time frame during field campaigns [Petetin et al., 2016; Zhang et al., 2013], or based on numerical simulations [Skyllakou et al., 2014]. Our study is a data-driven regional approach and considers a longer time period to study the seasonal/inter-annual variabilities of NH_3 and its impact of $PM_{2.5}$ formation over the Paris megacity. Specifically in this paper we study concentrations and

spatiotemporal variability of atmospheric NH_3 from the agricultural sector to gain insights on its effects on megacity air quality using: 1) long-term satellite observations derived from IASI (10 years from 2008 to 2017) and CrIS (5 years from 2013 to 2017) at regional scale (400km radius-circle from Paris city center); 2) spatiotemporal patterns of the CHIMERE model evaluated against the IASI and CrIS datasets for 2014 and 2015; and 3) the main meteorological parameters favoring the secondary $PM_{2.5}$ formation from NH_3 in the Paris megacity are analyzed.

2. Methodology

2.1. Region of analysis

The domain of analysis covers a circular area of 400 km radius around the Paris city center (Figure 1, larger circle) enabling the study of temporal and spatial variabilities of NH_3 emission sources likely to affect air quality in the Paris megacity. It has been selected for two reasons. First, it includes main regions known for their high NH_3 emissions, which can be transported and affect air quality over the Parisian region (Ile-de-France –IdF-, smaller circle in Figure 1). Emission regions in the Netherlands, North of Germany, Northwest of Belgium, and the Brittany region in France, are highlighted in darker colors in Figure 1 (emissions values are from the European Monitoring and Evaluation Programme -EMEP- 2015). Second, this area corresponds to the transport of 24 hours back-trajectories from Paris generated from the HYSPLIT model for one year, ensuring that NH_3 can indeed be efficiently transported from the emitting sources within the selected domain to the IdF region.

2.2. Satellite observations of ammonia

For this study we used the available date from IASI and CrIS which are both Fourier transform spectrometers to evaluate the current capacity to observe NH_3 concentrations from space, and study its variability around IdF. Technical information are summarized in Table 1.

2.2.1. Infrared Atmospheric Sounding Interferometer (IASI)

IASI is a nadir-viewing spectrometer launched on board the Metop-A and Metop-B satellites and operated by EUMETSAT (European Organisation for the Exploitation of Meteorological Satellites), since October 2006 and September 2012, respectively. These satellites are on similar polar orbits with Equator crossing times at 09:30 (21:30) local mean solar time for the descending (ascending) orbit. IASI measures the thermal infrared radiation of the system Earth-atmosphere in the spectral range from 645 to 2760 cm^{-1} with a spectral resolution 0.5 cm^{-1} apodized. The satellite swath is an area of 2200 km width composed by off-nadir measurements up to 48.3° on both sides of the track. At nadir, the IASI field of view is composed of 4 x 4 pixels of 12 km diameter each [Clerbaux et al., 2009].

The NH_3 total columns used here are derived from IASI using an Artificial Neural Network reanalyzed with ERA-interim data (ANNI-NH3-v2.1R [Van Damme et al., 2017]). This dataset is consistent in time and suitable for investigating inter-annual variability, which is one purpose of this study. Note that we have considered here only morning measurements (9:30) since the evening ones (21:30) are associated with larger relative errors [Van Damme et al., 2017]. IASI retrievals provide a robust error estimate for each IASI-NH3 observations, allowing to take into account the variable sensitivity when comparing IASI dataset with independent measurements. Finally, no filter on relative errors of the IASI datasets has been applied following recommendations from Van Damme et al. (2017) and outliers for which concentrations exceed 10 standard deviations above the mean in the domain of study have been removed.

Over the studied area, Metop-A and Metop-B have an overpass time difference ranging from only a few seconds to 67 minutes depending on the viewing geometry of the satellite scans; the average difference is 26 minutes for the 1325 days of common measurements. Monthly maps for the 10 years of observations between 2008 and 2017 are obtained by averaging Metop-A and whenever Metop-B (the two instruments are considered jointly for their period of common operation from March 2013 to 2017) with more than 10^5 pixels on average over the domain of analysis. The number of available NH_3 columns depends not only on the satellite overpass time but also on the state of the atmosphere being remotely sensed (e.g. thermal contrast and cloud cover). IASI NH_3 has been evaluated using the LOTOS-EUROS model over Europe [Van Damme et al., 2014b] and ground-based and airborne measurements [Van Damme et al., 2015b], showing consistency between the IASI NH_3 and the available datasets. When comparing IASI NH_3 (previous IASI-NN version) with ground-based Fourier transform infrared (FTIR) observations, a correlation of 0.8 and a slope of 0.73, with a mean relative difference of −32.4 ± (56.3)% have been found [Dammers et al., 2016].

2.2.2. Cross-track Infrared Sounder (CrIS)

The CrIS instrument [Zavyalov et al., 2013] is a Fourier Transform spectrometer operated by the Joint Polar Satellite System (JPSS) program on Suomi National Polar-orbiting Partnership (NPP) satellite, launched on 28 October 2011. CrIS is in a sun-synchronous orbit with a mean local daytime overpass time of 13:30 (01:30) in the ascending (descending) node. CrIS measures the atmospheric composition over three wavelength bands in the infrared region (645–1095 cm^{-1}; 1210–1750 cm^{-1}; 2155–2550 cm^{-1}). NH_3 retrievals are performed from the 645–1095 cm^{-1} band with a spectral resolution of 0.625 cm^{-1}. The CrIS instrument scans a 2200 km swath width (+/- 50 °). At nadir, the CrIS field of view consists of a 3 × 3 array of circular pixels of 14 km diameter each.

The CrIS Fast Physical Retrieval (CRPR) [Shephard and Cady-Pereira., 2015] uses an optimal estimation approach [Rodgers, 2000] that minimizes the difference between the CrIS measured

187 atmospheric spectra and a very fast Optimal Spectral Sampling (OSS) [Moncet et al., 2008]
188 forward model simulated spectrum to retrieve atmospheric profiles of ammonia volume mixing
189 ratios. This physical approach provides direct estimates of the retrieval errors and the vertical
190 sensitivity (averaging kernels) of the satellite observations, which is important as they vary from
191 profile-to-profile depending on the atmospheric state. The retrieved error covariance and
192 averaging kernels are also beneficial for air quality model comparisons and data assimilation
193 into models as any *a priori* information used in the retrieval can be accounted for in a robust
194 manner (i.e. observation operator). CrIS has been shown to retrieve ammonia surface
195 concentrations values down to ~0.2-0.3 ppbv under favorable conditions [Kharol, et al., 2018].
196 CrIS comparisons with ground-based FTIR observations show a correlation of 0.77 with a low
197 CrIS bias of +2% in the total column [Dammers et al., 2017]. Initial evaluation against surface
198 observations from the Ammonia Monitoring Network (AMoN) show that even with the inherent
199 sampling differences between the two surface observations they compare well with a
200 correlation of 0.76 and an overall mean CrIS – AMoN difference of ~+15% [Kharol et al., 2018].

201 For this study, the CrIS quality flag = 4 has been used, ensuring that retrievals provide some
202 information from the measurement (degrees-of-freedom- of-signal > 0.1). In addition, outliers
203 for which concentrations exceed 10 standard deviations above the mean have been removed.

204 ### 2.3. Modelling NH_3 from the CHIMERE model

205 The CHIMERE runs used in this study were obtained in the framework of the Copernicus
206 Atmospheric Monitoring Service (CAMS, https://atmosphere.copernicus.eu/), and its annual
207 task devoted to the production of regional reanalysis over Europe. The hindcasts for year 2014
208 and 2015 (raw simulation without data assimilation) were produced over Europe with a
209 horizontal resolution of 0.1° per 0.1° and
210 9 vertical levels stretched from the surface up to 500 hPa (~5000m). The input data to feed
211 CHIMERE [Menut et al., 2013; Mailler et al., 2017] were the Integrated Forecasting System (IFS)
212 meteorological data from European Centre for Medium-Range Weather Forecasts (ECMWF), the
213 annual emission inventory provided by the Netherlands Organisation for Applied Scientific
214 Research (TNO) [Kuenen et al., 2014] for year 2011 and the fire emissions from the Global Fire
215 Assimilation System (GFAS, [Kaiser et al., 2012]).The model computes hourly concentrations for
216 more than 180 species, among which are the regulated pollutants such as ozone, PM_{10}, and
217 NH_3. Within CHIMERE a comprehensive modelling system allows to compute the evolutions of
218 gaseous species and aerosols taking into account physical and chemical process. More than 30
219 gaseous species are involved in the chemical scheme and an aerosol module assesses the gas-
220 particulate phase equilibrium and compute the aerosol composition (inorganic, organic and
221 natural components).These datasets were evaluated over Europe for several pollutants before
222 being used for air quality studies (http://policy.atmosphere.copernicus.eu/Reports.html).

The model NH_3 profiles were integrated vertically along the 9 km model layers to provide a column that can be compared to that of the satellite measurements. Concretely this makes the reasonable assumption that all the NH_3 is located within this 0-5km layer (see e.g. Figure 1 in [Whitburn et al., 2016]).

2.4. Relative scales and coincidence criteria for dataset comparisons

Direct quantitative comparisons of satellite NH_3 products are difficult because of the different overpass times and ground footprint sizes of the 2 space borne instruments, which are not compatible with the high variability of NH_3 in space and time. Therefore, the evaluation of satellite observations is often made with the use of in situ measurements performed at surface and onboard aircrafts [Nowak et al., 2012; Van Damme et al., 2015b], or with ground-based remote-sounding FTIR [Dammers et al., 2016; Dammers et al., 2017].

The purpose here of comparing CrIS and IASI is to assess qualitatively the spatiotemporal patterns of the NH_3 sources derived from the two datasets and use these regional observations to evaluate the CHIMERE model in the domain of analysis at the local time for their respective overpasses: 9:30 and 13:30. CHIMERE outputs, in terms of NH_3 concentrations, have already been compared to the IASI observations at regional scale (Europe, [Fortems-Cheiney et al., 2016], and to surface measurements at local scale (Paris, [Petetin et al., 2016]), but have never been evaluated against the CrIS observations.

One aspect that needs to be considered when comparing concentration amounts inferred from infrared satellite observations is the importance of the algorithm and the a priori information used in the retrieval, especially for NH_3 which has limited vertical information. Some differences between the IASI and CrIS observations might arise due to instrument measurement differences (e.g. sensitivity), difference sampling period (e.g. overpass times of morning/evening vs middle of day/night), and retrieval algorithm differences, but they have both been validated and shown to capture well the spatiotemporal variations in lower tropospheric ammonia. Since the purpose of our study is not to quantitatively compare IASI and CrIS NH_3 data, but rather to use these independent datasets to assess NH_3 sources patterns over the domain and qualitatively evaluate the CHIMERE model in term of NH_3 concentrations and variabilities, a standardization procedure was applied to their retrieved absolute NH_3 columns. We computed “standardized columns” for each independent dataset (IASI, CrIS, and CHIMERE, separately) for 2014 and 2015 over the domain of study in such a way that the corresponding values have a standard deviation of 1 and a mean of 0, as in [Wilks, 2011].

In addition, to compare CHIMERE outputs with satellite data/columns, spatial and temporal coincidence criteria have been applied. To compare satellite observations, all CrIS pixels located within a 25-km radius circle from the center of the IASI ground pixels have been considered

within the same day of measurements. A spatial criterion of 25 km has been chosen because it optimizes the number of pairs involved in the statistics and improves the correlations. As for the comparisons between the model and the observations: all CHIMERE outputs located within the same 0.15°x0.15° grid box than the satellite and within 1 hour from its measurement have been selected.

3. Results

3.1. NH_3 regional observations derived from IASI (10-years) and CrIS (5-years)

3.1.1. Seasonal variabilities

First the seasonal variability was investigated over the IdF area. On a monthly basis, the 10-year and 5-year averaged regional NH_3 total column distributions derived from IASI and CrIS were found to exhibit a high seasonality over the domain (Figures 2 and 3). Note that the distributions in Figures 2 and 3 have been obtained by averaging satellite NH_3 observations in 0.25°x 0.25° grid boxes. Both satellite datasets exhibits the same variability over the domain even if the time period is different (10-years versus 5-years) and the sampling hour differs (~9.30 versus ~13.30). One note that CrIS and IASI NH_3 columns present small differences in term of NH_3 total columns in low concentration regimes in the domain of study.

In these figures (2 and 3) high NH_3 concentrations (up to 2.10^{16} molecules/cm^2) can be observed from March to August at different locations of the domain:

- The French Champagne-Ardennes region in March and April (Figures 2 and 3, box A),
- The northern part of the domain corresponding to the Netherlands and the North of Belgium from April to August (Figures 2 and 3, box B), and
- The Brittany/Pays de la Loire regions (West of France) mainly in April and August but still persistent from March to August (Figures 2 and 3, box C).

The observed seasonality is related to agricultural practices (fertilizer application period varying as function of the crop types and farming species) and changes in temperatures, with higher temperatures favoring volatilization. This explains the high concentration in July and August.

In the Champagne-Ardennes region, areas of hotspots do not correspond to vineyards but to field vegetables and root crops (from the Institut National de la Recherche Agronomique INRA https://odr.inra.fr/intranet/carto/cartowiki/index.php/OTEX_et_Orientation_Agricole_des_territoires, and AGRESTE, Service Central d'Enquêtes et d'Études Statistiques, 2015 http://agreste.agriculture.gouv.fr/IMG/pdf/R4215A15.pdf). This is a leader region for mineral fertilization used for sugar industry in France [Ramanantenasoa et al., 2018]. Hamaoui-Laguel et al. (2014) and Fortems-Cheiney et al. (2016) have previously noted that NH_3 emissions in this

region, mainly due to fertilizer over barley, sugar beet, and potato starch in early March, were higher than what have been reported in the EMEP inventory.

NH_3 concentrations are high from April to August in the northern part of the domain that is known for its animal farming (Eurostat 2014, http://ec.europa.eu/eurostat/statistics-explained/index.php?title=File:Livestock_density_by_NUTS_2_regions,_EU-28,_2013.png, [Van Damme et al., 2014a]).

In the Pays de la Loire, NH_3 concentrations are high in April and August and remain relatively high from March to September. Hotspots are found in areas of livestock farming, mainly poultry and granivorous, which explains the high and relatively constant NH_3 concentrations over warmer periods in this region.

3.1.2. Inter-annual variabilities

As can be seen in Figures 2 and 3, NH_3 concentrations are enhanced between March and August in the domain. In this section, inter-annual variabilities are discussed regarding meteorological conditions and agricultural practices during this time period.

Inter-annual variability of NH_3 is higher in springtime than in summer, e.g. in June the variance is 8 times lower than for the other months. To illustrate the inter-annual variability in springtime, maps of monthly mean NH_3 total columns derived in March-April period from IASI (2008-2017 time period) and from CrIS (2013-2017 time period) are shown in Figure 4. Both satellite distributions exhibit the same inter-annual variability from 2013 to 2017 with higher NH_3 concentrations in 2015 over the northern part of the domain than the other years. NH_3 concentrations derived from IASI in 2011 are 150% higher in spring (March and April) compared to 2016 (Figure 4). This inter-annual variability is partly driven by meteorological conditions and specific agricultural constrains (crop type and phenological stage for instance).

To investigate the impact of meteorological conditions on atmospheric NH_3 variability, we computed the monthly mean anomalies of total precipitation versus skin temperature derived from ECMWF ERA-interim [Dee et al., 2011], color coded by NH_3 total columns anomalies derived from IASI, as shown in Figure 5. Monthly mean anomalies have been calculated relative to the 10-years averages (in %). In this figure, monthly NH_3 total columns are at least 10% higher (positive anomalies, red dots) when skin temperatures are higher and total precipitation are lower than the 10-year average. In contrast, negative monthly NH_3 total columns anomalies (blue dots, Figure 5) are associated with higher total precipitation and lower skin temperatures than the 10-years average. To further detail this analysis, Figure 1 of the supplement information shows bar plots of monthly mean NH_3 total columns derived from IASI, total precipitation and skin temperature derived from ECMWF from March to August, plotted in different colors for the different years of measurements from 2008 to 2017. NH_3 total columns

are larger by more than 300% in March-April 2012 compared to 2013 (Figure S1a). Total precipitation is higher (0.4 mm compared to 1 mm, Figure S1b) and skin temperature is lower (281 compared to 288 K, Figure S1c) in March 2013 than in March 2012 on average over the domain. Overall, total precipitation is anti-correlated with NH_3 concentrations in the atmosphere (R = -0.52 from March to August for all years, not shown here) because of a) the wet deposition importance in the atmospheric NH_3 removal and b) the absence of fertilization during rainy periods. Skin temperature is relatively correlated with NH_3 concentrations (R = 0.33 from March to August for all years) since higher temperature increases volatilization of NH_3 from the surface to the atmosphere.

In addition, NH_3 concentration is maximum in March 2011 whereas it peaks later in April for 2012 (Figure S1a). Springtime is a spreading fertilizer period depending on many agricultural and meteorological constrains. When temperature are mild, such as in 2012 (Figure S1b), fertilizer spreading occurs sooner because the phenological growth stage is more advanced. Fertilizing process period also varies in function of the sowing date which depends on agricultural practices and crop types: corn is fertilized in early spring whereas rapeseed is in late spring.

Overall, all these meteorological (precipitation and temperature) and agricultural (fertilizer and manure applications) parameters account for the high NH_3 inter-annual variabilities revealed by both IASI and CrIS in the domain of study.

3.2. Comparisons of NH_3 columns derived from IASI, CrIS, and CHIMERE for 2014 and 2015

To discuss the representation of agricultural emissions in the models in terms of intensity and both spatial and temporal distributions, regional satellite observations derived from IASI and CrIS have been compared to the CHIMERE model in the region of analysis.

3.2.1. Annual cycle

Standardized monthly mean concentrations derived from IASI, CrIS, and CHIMERE for 2014 and 2015 are shown in Figure 6. These years were selected as NH_3 total columns were found to vary a lot, reaching 10% higher in March and 50% lower in May than the 10-years average

As can be seen from the plot, the 3 datasets exhibit similar patterns in terms of seasonality: all are enhanced in March-April and in summer, and show a decrease in May. However two major differences can be noted. First, CrIS standardized NH_3 columns are higher in winter (November, December, and January) compared to the other dataset which can be also be seen in Figure 3. This could be attributed to a higher number of outliers, given the larger standard deviation (shaded areas, Figure 6) and no attempt to account for potential non-detects when concentrations fall below the instrument detection limits. For these months, NH_3 levels are low

and undetectable by satellite observations (Figures 2 and 3) so these high values could be interpreted as observational noise. The detection limit depends on the instrument characteristics and atmospheric state, with IASI minimum detection limit of ~2-3 ppbv (~4-6.10^{15} molecules.cm^{-2}) [Clarisse et al., 2010] and CrIS ~0.5-1.0 ppbv (~1-2.10^{15} molecules.cm^{-2}) [Shephard and Cady-Pereira, 2015; Kharol et. al., 2018]. Second, the CHIMERE standardized NH_3 columns are enhanced in September 2014, which is not supported by the observations. It has been recently shown that CHIMERE overestimated NH_3 emissions in autumn over Europe [Couvidat et al., 2018]. Generally, the amplitude of the modelled seasonal cycle exceeds the measured ones, which could be explained by higher concentrations measured in winter due to the observational noise and lower emissions.

Over the whole period, the coefficient of determination (r^2) between the standardized monthly mean NH_3 columns derived from IASI (CrIS), and the CHIMERE model is 0.58 (0.18) for the annual cycles of 2014 and 2015 (not shown here). If we only consider months of high NH_3 in the domain from March to August, the correlation between the observational datasets and the model is good with linear regression slope values between IASI (CrIS) and CHIMERE of 0.98 (0.71), as shown in Figure 7. The seasonal cycle is thus well reproduced by the model, which is encouraging given the fact that annual total emissions are simply disaggregated with a monthly profile in the model. However, the values of the r^2 lower than 0.5 indicate that the CHIMERE model only reproduces at most half of the observed monthly temporal NH_3 variabilities in the domain. Similar variabilities are found between the observations and the model outputs since the coefficients of correlation of the standard deviations are 0.4 and 0.6 between CHIMERE and IASI and CrIS, respectively.

3.2.2. Spatial variability of NH_3 in springtime

The IASI and CrIS regional maps have been compared to the CHIMERE model for the March-April period in 2014 and 2015 to evaluate the model's capacity to reproduce the spatial distribution of the episodic emissions from fertilizer spreading practices in springtime, as well as their inter-annual variability. Satellite NH_3 measurements in springtime have been gridded at 0.15°x 0.15° spatial resolution, and the associated CHIMERE maps have been computed following the coincident criteria described in section 2.4 at the same spatial resolution (Figures 8 and 9).

First one can notice that the spatial distribution of NH_3 observed in springtime by both satellite instruments are in good agreement, even though their overpass time is different (~4 hours apart). This was already seen in the inter-annual variability agreement seen in Figure 4. In spring 2014, IASI and CrIS both reveal three main regions of enhanced NH_3 concentrations (North, Champagne-Ardennes, and Brittany/Pays de la Loire region) already identified by the 10-years and 5-years of IASI and CrIS observation maps (Boxes A, B, and C of Figures 2 and 3). In 2015, concentrations of NH_3 in the northern part of the domain are higher than in 2014, as indicated

by both IASI and CrIS observations (Figure 9, upper panels). Overall, satellite observations are able to capture similar spatial distributions of high NH_3 concentrations in springtime, and their evolution in time.

In spring 2014, the CHIMERE model reproduces the high concentrations in the three regions of the domain identified in Figures 2 and 3. Additional NH_3 hot spots in the southeastern part of the domain including the Po Valley, Switzerland, and the wine region between Besancon and Lyon (blue box in Figure 8) are indicated by the CHIMERE model. NH_3 emissions in this latter region are comparable to average agricultural plains over France. Only dispersion conditions related to wind speed and boundary layer height can explain high NH_3 concentrations over this area.

In spring 2015, satellite observations and the CHIMERE model outputs exhibit very similar patterns in term of high NH_3 distributions, with however higher NH_3 concentrations indicated by the model in the southern part of the domain (blue box in Figure 9).

Finally, the (model - observations) differences between the standardized NH_3 column derived from the satellite instruments in springtime 2014-2015 and the corresponding NH_3 columns derived from the CHIMERE model are shown in Figure 2 of the supplement information. One can see that very similar patterns are presented when comparing the model to independent satellite observations from IASI and CrIS: the modelled NH_3 concentrations are systematically lower for both years over Belgium and United Kingdom, and higher in the southern part of the domain (green square, Figure S2) including the Pays de la Loire region (box C in Figures 2 and 3), and in the southeastern part of the domain (over the North part of Switzerland and the Plateau du Jura region - between Besancon and Lyon cities – blue box in Figure 8). Reasons of enhanced NH_3 columns derived from the model in this latter region are not clear yet. An explanation could be that the temporal distribution of the emissions is misrepresented in the model since the modelled concentrations are enhanced in April whereas the two satellite observations are enhanced earlier in March for both years. It is worth noting that there are no EMEP stations measuring surface NH_3 concentrations in these regions. As for the Brittany/Pays de la Loire region, it has already been shown that the LOTOS-EUROS atmospheric model [Schaap et al., 2008] using similar chemistry schemes and NH_3 emissions shows higher columns each year in this area [Van Damme et al., 2014b].

3.3. Conditions for PM formation in the Paris megacity

To investigate the impact of intensive agriculture practices on the Paris megacity air quality, we need to better understand the role of NH_3 in the formation of $PM_{2.5}$ that depends, among others, on specific meteorological conditions such as atmospheric temperature and humidity that alter the gas-particle partitioning. The link between high NH_3 concentrations inducing $PM_{2.5}$

formation in the Paris megacity is known [Petetin et al., 2016; Zhang et al., 2013] but quantification of such phenomena is difficult due the lack of long-term NH_3 monitoring in the IdF region. $PM_{2.5}$ is however measured hourly at several locations in Paris by the Airparif network (https://www.airparif.asso.fr/, Figure 1). Thanks to the 10 years of IASI observations, an observational evidence of $PM_{2.5}$ formation in the IdF region (100 km around Paris - black box in Figure 1) is represented in Figure S3. Simultaneous enhancements in March of $PM_{2.5}$ measured at the surface and NH_3 columns derived from the IASI observations over the IdF region are clearly visible. However, high concentrations of NH_3 observed in summer are not associated with high $PM_{2.5}$ concentrations. This reflects the complexity of the $PM_{2.5}$ formation depending on various factors, such as NH_3 emissions, atmospheric chemistry (acidic content of the atmosphere), transport, and specific meteorological conditions involved in the gas to solid phase conversion between NH_3 and ammonium salts.

To evaluate the impact of long-range transport on NH_3 levels observed over the Parisian region (IdF) in spring, back-trajectory analysis was performed. In total 231 24-hours back-trajectories ending in Paris (period from February 15th to May 15th from 2013 to 2016) were classified into 8 clusters using HYSPLIT (https://ready.arl.noaa.gov/HYSPLIT.php). Figure 10 shows the mean trajectories for each cluster associated with the average NH_3 total columns measured by IASI over the IdF region. In this figure, higher NH_3 columns are found under the influence of air masses transported from the northern part of the domain (over Belgium and the Netherlands, clusters 4 and 5) and from the Brittany region (cluster 8), which are the major sources regions of NH_3 in spring in the domain as previously identified (Figures 2 and 3). Clusters 2 and 3 (Figure 10) are associated with intermediate NH_3 levels since air masses moved slowly transporting NH_3-rich air from rural regions near IdF (such as the Champagne-Ardennes region - Box A in Figures 2 and 3) to Paris. Finally, low NH_3 concentrations are measured when air masses originated from ocean regions passing through continental areas with minor NH_3 sources in spring (clusters 1, 6 and 7, Figure 10). This reflects the importance of long-range transport in the NH_3 budget observed over the Paris megacity in spring.

To quantitatively assess the influence of meteorological parameters on the formation of $PM_{2.5}$ from NH_3 in the IdF region, timeseries of NH_3 total columns, $PM_{2.5}$ surface concentrations, and four meteorological parameters (temperature at 2 m, boundary layer height, total precipitation and relative humidity) derived from ECMWF - ERA-Interim [Dee et al., 2011] were analyzed. To compute daily and monthly means, IASI NH_3 total columns have been averaged over IdF (black box in Figure 1), $PM_{2.5}$ concentrations measured between 9 AM and 11 AM have been averaged over the 14 stations (dark points in Figure 1), and ECMWF data have been averaged over a 300 km region around Paris (the blue box in Figure 1). Figure 11 shows all these parameters for spring 2014.

We have flagged pollution episodes in both time series ($PM_{2.5}$ and NH_3) by selecting data above 1-sigma standard deviation over the mean of the datasets from 2013 to 2016. This time period was selected to have enough IASI observations in the IdF region. Then two cases have been defined to study the temporal correlation between NH_3 and $PM_{2.5}$: case A in which both NH_3 and $PM_{2.5}$ pollution episodes appear simultaneously, i.e. within the same day or 2 days apart (shaded in red in Figure 11); case B in which pollution episodes appear at least 3 days apart (shaded in blue in Figure 11). In Figure 11, a strong relationship between peaks of NH_3, $PM_{2.5}$ and meteorological parameters can be seen. For example, between March 3rd and March 19th 2014 (case A), the boundary layer height is exceptionally low (456 m; compared to 760 m on average); the temperature is relatively low (280 K; 282 K on average); and there is no precipitation (0.01 mm/h; 0.11 mm/h on average). One note that peaks of maximum NH_3 observed in IdF on March 11th and 12th are associated with air masses coming from the northern part of the domain (clusters 4 and 5 in Figure 10). In contrast, for the case B in which appearance of peaks of NH_3 and $PM_{2.5}$ is not simultaneous, meteorological conditions are different: the boundary layer is thicker (908 m on April 23rd 2014), or temperature is higher (285 K on April 11th 2014).

To further investigate the influence of meteorological parameters on the pollution episodes in the IdF region, detailed analysis have been made over the whole dataset. Figure 12 shows the statistical distribution of meteorological parameters corresponding to case A, case B, and all observations. One can see that the boundary layer height is significantly lower in case A (550 ± 205 m) than in case B (751 ± 276 m), and that precipitations are absent in case A (0,019 mm/h) compared to case B (0,085 mm/h). The temperature at 2 meters also differs between the two cases (case A: 278 ± 3 K; case B: 282 ± 4 K), but the humidity is almost the same (70% ± 17% versus 75%±18%). Thus the combination of the following three meteorological parameters favors simultaneous appearances of NH_3 and of $PM_{2.5}$ in Paris (i.e. case A): low surface temperatures (5°C), with thin boundary layers (~500m), and rare precipitations. In addition, the Wilcoxon-Mann-Whitney test ([Wilks, 2011], not shown here) indicates that each single parameter has no significant influence on the NH_3-$PM_{2.5}$ correlation. Therefore only a combination of these different parameters has an impact on secondary aerosol formation from NH_3.

An explanation of these findings might be that anticyclonic conditions (low planetary boundary layer), preventing pollutant dispersions in the lower atmosphere [Salmond and McKendry, 2005], along with moderate wind fields allow NH_3 plumes to be transported from rural to urban regions [Petit et al., 2015]. In addition, thanks to relatively low atmospheric temperatures and a moderate relative humidity, conversion of gas phase NH_3 to ammonium salts is then accentuated via optimal phase equilibrium [Watson et al., 1994; Nenes et al., 1998]. Finally, with the absence of rain, ammonium salts are stabilized in the aerosols.

Our observations are in agreement with previous studies [Bessagnet et al., 2016; Wang et al., 2015], which have shown that the formation of ammonium salt needs a specific humidity of 60 - 70%, because it corresponds to the deliquescence point of NH_4NO_3 in ambient air. This is in agreement with our results since the mean of relative humidity in case A is 70%. Our results also support the idea that a relatively low atmospheric temperature favor $PM_{2.5}$ formation since the phase equilibrium leads to NH_4NO_3 decomposition above 30 °C.

4. Conclusions

This study focuses on seasonal and inter-annual variabilities of NH_3 concentrations in a 400 km radius-circle area around Paris to assess the evolution of major NH_3 agricultural sources and its key role in the formation of the secondary aerosols that affect air quality over the Paris megacity.

Thanks to 10-years and 5-years of regional NH_3 observations derived from IASI and CrIS, three main regions of high NH_3 occurring between March and August were identified. Observed inter-annual variabilities of NH_3 concentrations have been discussed with respect to total precipitations and atmospheric temperature, showing that total precipitations are anti-correlated with high NH_3 concentrations, and that mild temperature in late winter causes precocious fertilizer spreading due to advanced phenological growth stage.

To evaluate our knowledge on agricultural emissions in terms of intensity and both spatial and temporal distributions, coincident CHIMERE model outputs have been compared to satellite observations of IASI and CrIS for 2014 and 2015. The annual cycle is well reproduced by the model (correlation slopes of 0.98 and 0.71 between the model and IASI and CrIS, respectively) but the model is only able to reproduce half of the observed atmospheric NH_3 variability. Focusing on spring periods (March-April 2014 and 2015) of episodic NH_3 emissions, the two independent satellite observations derived from IASI and CrIS show very similar spatial distributions of high NH_3 concentrations, as well as their evolution in time. The comparison between CHIMERE NH_3 columns and coincident satellite observations highlights the same difference spatial patterns with a systematic underestimation of NH_3 concentrations from the model over Belgium and an overestimation in the southern part of the domain (French Brittany/Pays de la Loire and Plateau du Jura regions, as well as North of Switzerland).

Focusing on the Ile-de-France (IdF, 100 km around Paris) region, we found that air masses originated from rich-NH_3 areas, mainly the northern part of the domain over Belgium and the Netherlands, increase the observed NH_3 total columns measured by IASI over the urban area of Paris.

To assess the link between NH_3 and $PM_{2.5}$ over the Parisian (IdF) region, the main meteorological parameters driving the optimal conditions involved in the $PM_{2.5}$ formation have

been identified. The results show that relatively low temperature, thin boundary layer, coupled with almost no precipitation, favor the $PM_{2.5}$ formation with the presence of atmospheric NH_3 in the IdF region. Based on a more observational approach over large time scale, this work is in agreement with previous studies.

This study highlights the need for a better representative NH_3 monitoring to improve numerical simulation of spatial and temporal NH_3 variabilities, especially at fine scales. In order to compare IASI and CrIS data in absolute values, it would be recommended to derive both datasets using the same retrieval algorithm. Thus, by combining these datasets bi-daily NH_3 total columns in absolute values at regional scale would be provided. This would help inferring variability of top-down NH_3 emissions. Complementarily, long term quantification of NH_3 diurnal cycle inside Paris would improve comparisons with local $PM_{2.5}$ needed to understand secondary aerosols formations. For this purpose, an ongoing activity consists in the deployment of a mini-DOAS instrument [Volten et al., 2012] used for long-term and continuous monitoring of atmospheric NH_3 concentrations in the center of Paris from the QUALAIR platform (https://www.ipsl.fr/en/Our-research/Atmospheric-chemistry-and-air-quality/Tropospheric-chemistry/QUALAIR). Finally, the geostationary-orbit sounder IRS-MTG ([Stuhlmann et al., 2005], to be launched after 2022) will provide NH_3 columns at very high sampling rate (every 0.5 hour over Europe) with an unpreceded spatial resolution (pixel size of 4 km).

Author contribution:

CV wrote the paper with contributions of all coauthors. CV and CC designed the study. MV, LC, and SW performed IASI retrievals and ED, MWS, and KEC performed the CrIS retrievals. FM ran the CHIMERE simulations. CV and TW analyzed the data with guidance from CC and PFC. All authors discussed the results and contributed to the final paper.

Acknowledgement:

IASI is a joint mission of Eumetsat and the Centre National d'Etudes Spatiales (CNES, France). This work was supported by the CNES. It is based on observations with IASI embarked on Metop. The IASI Level-1C data are distributed in near real time by Eumetsat through the EumetCast system distribution. The authors acknowledge the Aeris data infrastructure (http://iasi.aeris-data.fr/NH3/) for providing access to the IASI Level-1C data and Level-2 NH_3 data used in this study. The French scientists are grateful to CNES (TOSCA) and Centre National de la Recherche Scientifique (CNRS) for financial support. The research in Belgium is also funded by the Belgian State Federal Office for Scientific, Technical and Cultural Affairs and the European Space Agency (ESA Prodex IASI Flow project). The CrIS Fast Physical Retrieval (CFPR) NH_3 data is provide through a joint collaboration between Environment and Climate Change Canada (ECCC) and Atmospheric and Environmental Research (AER), Inc. (USA). The Level 1 and Level 2 input data for CFPR were obtained from the University of Wisconsin-Madison Space Science and

Engineering Center (SSEC) and the NOAA Comprehensive Large Array-Data Stewardship System (CLASS) (Liu et al.,2014), with special thanks to Axel Graumann (NOAA).

References

Battye, W., Aneja, V. P., and Schlesinger W. H.: Is nitrogen the next carbon?, Earth's Future, 5, 894–904, doi:10.1002/2017EF000592, 2017.

Beer, R., Shephard, M. W., Kulawik, S. S., Clough, S. A., Eldering, A., Bowman, K. W., Sander, S. P., Fisher, B. M., Payne, V. H., Luo, M., Osterman, G. B., and Worden, J. R.: First satellite observations of lower tropospheric ammonia and methanol, Geophys. Res. Lett., 35, L09801, doi:10.1029/2008GL033642, 2008.

Behera, S. N., Sharma, M., Aneja, V. P., and Balasubramanian, R.: Ammonia in the atmosphere: a revieon emission sources, atmospheric chemistry and deposition on terrestrial bodies, Environ. Sci. Pollut. Res. Int., 20, 8092-8131, doi: 10.1007/s11356-013-2051-9, 2013.

Bessagnet, B., Meleux, F., Favez, O., Beauchamp, M., Colette, A., Couvidat, F., Rouïl, L., Menut, L. : Le rôle de l'agriculture sur les concentrations en particules dans l'atmosphère et l'apport de la modélisation (the role of agriculture on the concentrations of particles in the atmosphere and supply modeling), Pollution atmosphérique, climat, santé, société, 229–230, 154–165, 2016.

Bey, I., Jacob, D. J., Yantosca, R. M., Logan, J. A., Field, B., Fiore, A. M., Li, Q., Liu, H., Mickley, L. J., and Schultz, M.: Global modeling of tropospheric chemistry with assimilated meteorology: Model description and evaluation, J. Geophys. Res., 106, 23,073-23,096, 2001.

Clerbaux, C., Boynard, A., Clarisse, L., George, M., Hadji-Lazaro, J., Herbin, H., Hurtmans, D., Pommier, M., Razavi, A., Turquety, S., Wespes, C., and Coheur, P.-F.: Monitoring of atmospheric composition using the thermal infrared IASI/MetOp sounder, Atmos. Chem. Phys., 9, 6041–6054, doi:10.5194/acp-9-6041-2009,2009

CEIP, Centre on Emission Inventories and Projections, 'EMEP officially reported emission data', http://www.ceip.at/ms/ceip_home1/ceip_home/webdab_emepdatabase/reported_emissionda ta/, last access July 2018.

CITEPA, Centre Interprofessionnel Technique d'Etudes de la Pollution Atmosphérique, Format SECTEN, https://www.citepa.org/fr/air-et-climat/polluants/aep-item/ammoniac, last access April 2018.

606 Clarisse, L., Clerbaux, C., Dentener, F., Hurtmans, D., and Coheur, P.-F.: Global ammonia
607 distribution derived from infrared satellite observations, Nat. Geosci., 2, 479–483,
608 https://doi.org/10.1038/ngeo551, 2009.

609 Clarisse, L., Shephard, M., Dentener, F., Hurtmans, D., Cady-Pereira, K., Karagulian, F., Van
610 Damme, M., Clerbaux, C., and Coheur, P.-F.: Satellite monitoring of ammonia: A case study of
611 the San Joaquin Valley, J. Geophys. Res., 115, D13302, https://doi.org/10.1029/2009JD013291,
612 2010.

613 Couvidat, F., Bessagnet, B., Garcia-Vivanco, M., Real, E., Menut, L., and Colette, A.: Development
614 of an inorganic and organic aerosol model (CHIMERE 2017*β* v1.0): seasonal and spatial
615 evaluation over Europe, Geosci. Model Dev., 11, 165-194, https://doi.org/10.5194/gmd-11-165-
616 2018, 2018.

617 Corso, M. Medina, S., and Tillier, C. : Quelle est la part des pics de pollution dans les effets à
618 court terme de la pollution de l'air sur la santé dans les villes de France ? Saint-Maurice: Santé
619 publique France, ISBN : 979-10-289-0259-9, 2016.

620 Dammers, E., Palm, M., Van Damme, M., Vigouroux, C., Smale, D., Conway, S., Toon, G. C.,
621 Jones, N., Nussbaumer, E., Warneke, T., Petri, C., Clarisse, L., Clerbaux, C., Hermans, C., Lutsch,
622 E., Strong, K., Hannigan, J. W., Nakajima, H., Morino, I., Herrera, B., Stremme, W., Grutter, M.,
623 Schaap, M., Wichink Kruit, R. J., Notholt, J., Coheur, P.-F., and Erisman, J. W.: An evaluation of
624 IASI-NH3 with ground-based Fourier transform infrared spectroscopy measurements, Atmos.
625 Chem. Phys., 16, 10351–10368, https://doi.org/10.5194/acp-16-10351-2016, 2016.

626 Dammers, E., Shephard, M. W., Palm, M., Cady-Pereira, K., Capps, S., Lutsch, E., Strong, K.,
627 Hannigan, J. W., Ortega, I., Toon, G. C., Stremme, W., Grutter, M., Jones, N., Smale, D., Siemons,
628 J., Hrpcek, K., Tremblay, D., Schaap, M., Notholt, J., and Erisman, J. W.: Validation of the CrIS fast
629 physical NH3 retrieval with ground-based FTIR, Atmos Meas Tech, 10, 2645-2667, 10.5194/amt-
630 10-2645-2017, 2017.

631 Dee, D. P., Uppala, S. M., Simmons, A. J., Berrisford, P., Poli, P., Kobayashi, S., Andrae, U.,
632 Balmaseda, M. A., Balsamo, G., Bauer, P., Bechtold, P., Beljaars, A. C. M., van de Berg, L., Bidlot,
633 J., Bormann, N., Delsol, C., Dragani, R., Fuentes, M., Geer, A. J., Haimberger, L., Healy, S. B.,
634 Hersbach, H., Hólm, E. V., Isaksen, L., Kållberg, P., Köhler, M., Matricardi, M., McNally, A. P.,
635 Monge-Sanz, B. M., Morcrette, J.-J., Park, B.-K., Peubey, C., de Rosnay, P., Tavolato, C., Thépaut,
636 J.-N. and Vitart, F.: The ERA-Interim reanalysis: configuration and performance of the data
637 assimilation system. Q.J.R. Meteorol. Soc., 137: 553–597. doi: 10.1002/qj.828, 2011.

638 Erisman, J. W., Sutton, M. A., Galloway, J. N., Klimont, Z., and Winiwarter, W.: How a century of
639 ammonia synthesis changed the world, Nat. Geosci., 1, 636–639, doi:10.1038/ngeo325, 2008.

640 Fortems-Cheiney, A., Dufour, G., Hamaoui-Laguel, L., Foret, G., Siour, G., Van Damme, M.,
641 Meleux, F., Coheur, P.-F., Clerbaux, C., Clarisse, L., Favez, O., Wallasch, M., and Beekmann, M.:
642 Unaccounted variability in NH3 agricultural sources detected by IASI contributing to European
643 spring haze episode, Geophys. Res. Lett., 43, 5475–5482, doi:10.1002/2016GL069361, 2016.

644 Fuzzi, S., Baltensperger, U., Carslaw, K., Decesari, S., Denier van der Gon, H., Facchini, M. C.,
645 Fowler, D., Koren, I., Langford, B., Lohmann, U., Nemitz, E., Pandis, S., Riipinen, I., Rudich, Y.,
646 Schaap, M., Slowik, J. G., Spracklen, D. V., Vignati, E., Wild, M., Williams, M., and Gilardoni, S.:
647 Particulate matter, air quality and climate: lessons learned and future needs, Atmos. Chem.
648 Phys., 15, 8217-8299, https://doi.org/10.5194/acp-15-8217-2015, 2015.

649 Galloway, J. N., Aber, J. D., Erisman, J. W., Seitzinger, S. P., Howarth, R. W., Cowling, E. B., and
650 Cosby, B. J.: The Nitrogen Cascade, BioScience, 53, doi: 10.1641/0006-3568(2003), 2003.

651 Gong, L., Lewicki, R., Griffin, R.J., Tittel, F.K., Lonsdale, C.R., Stevens, R.G., Pierce, J.R., Malloy,
652 Q.G.J., Travis, S.A., Bobmanuel, L.M., Lefer, B.L., and Flynn, J.H.: Role of atmospheric ammonia in
653 particulate matter formation in Houston during summertime, Atmos. Environ, 77: 893–900,
654 https://doi.org/10.1016/j.atmosenv.2013.04.079, 2013.

655 Hamaoui-Laguel, L., Meleux, F., Beekmann, M., Bessagnet, B., Génermont, S., Cellier, P.,
656 Létinois, L..: Improving ammonia emissions in air quality modelling for France, Atmos. Environ.,
657 92, 584–595, doi:10.1016/j.atmosenv.2012.08.002, 2014.

658 Heald, C.L., Collett Jr., J.L., Lee, T., Benedict, K.B., Schwandner, F.M., Li, Y., Clarisse, L., Hurtmans,
659 D.R., Van Damme, M., Clerbaux, C., Coheur, P.-F., Philip, S., Martin, R.V., and Pye, H.O.T.:
660 Atmospheric ammonia and particulate inorganic nitrogen over the United States, Atmos. Chem.
661 Phys., 12, 10295–10312, doi:10.5194/acp-12-10295-2012, 2012.

662 Holland, E.A., Bertman, S.B., Carroll, M.A., Guenther, A.B., Shepson, P.B., Sparks, J.P., and Lee-
663 Taylor, J.: U.S. Nitrogen Science Plan Focuses Collaborative Efforts, Eos. Trans. Am. Geophys.
664 Union., 86(27), 253-260, 2005.

665 Kaiser, J. W., Heil, A., Andreae, M. O., Benedetti, A., Chubarova, N., Jones, L., Morcrette, J.-J.,
666 Razinger, M., Schultz, M. G., Suttie, M., and van der Werf, G. R.: Biomass burning emissions
667 estimated with a global fire assimilation system based on observed fire radiative power. BG,
668 9:527-554, 2012.

669 Kharol, S. K., M. W. Shephard, C. A. McLinden, L. Zhang, C. E. Sioris, J. M. O'Brien, R. Vet, K. E.
670 Cady-Pereira, E. Hare, J. Siemons, and N. A. Krotkov.: Dry deposition of reactive nitrogen from
671 satellite observations of ammonia and nitrogen dioxide over North America, Geophysical
672 Research. Letters, 45, 1157-1166, https://doi.org/10.1002/2017GL075832, 2018.
673

674 Kranenburg, R., Hendriks, C., Kuenen, J., and Schaap, M.: Improved Modelling of Ammonia by
675 Using Manure Transport Data, In International Technical Meeting on Air Pollution Modelling and
676 its Application (pp. 483-486). Springer, Cham, December 2016.
677
678 Kuenen, J. J. P., Visschedijk, A. J. H., Jozwicka, M., and Denier van der Gon, H. A. C.: TNO-
679 MACC_II emission inventory; a multi-year (2003–2009) consistent high-resolution European
680 emission inventory for air quality modelling, Atmos. Chem. Phys., 14, 10963-10976,
681 https://doi.org/10.5194/acp-14-10963-2014, 2014.
682
683 Li, Y., Thompson, T. M., Van Damme, M., Chen, X., Benedict, K. B., Shao, Y., Day, D., Boris, A.,
684 Sullivan, A. P., Ham, J., Whitburn, S., Clarisse, L., Coheur, P.-F., and Collett Jr., J. L.: Temporal and
685 spatial variability of ammonia in urban and agricultural regions of northern Colorado, United
686 States, Atmos. Chem. Phys., 17, 6197-6213, https://doi.org/10.5194/acp-17-6197-2017, 2017.
687
688 Mailler, S., Menut, L., Khvorostyanov, D., Valari, M., Couvidat, F., Siour, G., Turquety, S., Briant,
689 R., Tuccella, P., Bessagnet, B., Colette, A., Letinois, L., and Meleux, F.: CHIMERE-2017: from
690 urban to hemispheric chemistry-transport modeling, Geosci. Model Dev., 10, 2397-2423,
691 https://doi.org/10.5194/gmd-10-2397-2017, 2017.

692 Menut, L., Bessagnet, B., Khvorostyanov, D., Beekmann, M., Blond, N., Colette, A., Coll, I., Curci,
693 G., Foret, G., Hodzic, A., Mailler, S., Meleux, F., Monge, J.L., Pison, I., Siour, G., Turquety, S.,
694 Valari, M., Vautard, R., and Vivanco, M.G.: CHIMERE 2013: a model for regional atmospheric
695 composition modelling, Geosci. Model Dev, 6, 981-1028, doi:10.5194/gmd-6-981-2013, 2013.

696 Moran, M. D., Dastoor, A., and Morneau, G.: Long-Range Transport of Air Pollutants and
697 Regional and Global Air Quality Modelling. In: Taylor E., McMillan A. (eds) Air Quality
698 Management, Springer, Dordrecht, 2014.

699 Moncet, J.-L, Uymin G., Lipton A. E., and Snell H. E.: Infrared radiance modeling by optimal
700 spectral sampling, J. Atmos. Sci., 65, 3917-3934, https://doi.org/10.1175/2008JAS2711.1, 2008.

701 Myhre, G., Samset, B. H., Schulz, M., Balkanski, Y., Bauer, S., Berntsen, T. K., Bian, H., Bellouin,
702 N., Chin, M., Diehl, T., Easter, R. C., Feichter, J., Ghan, S. J., Hauglustaine, D., Iversen, T., Kinne,
703 S., Kirkevåg, A., Lamarque, J.-F., Lin, G., Liu, X., Lund, M. T., Luo, G., Ma, X., van Noije, T., Penner,
704 J. E., Rasch, P. J., Ruiz, A., Seland, Ø., Skeie, R. B., Stier, P., Takemura, T., Tsigaridis, K., Wang, P.,
705 Wang, Z., Xu, L., Yu, H., Yu, F., Yoon, J.-H., Zhang, K., Zhang, H., and Zhou, C.: Radiative forcing of
706 the direct aerosol effect from AeroCom Phase II simulations, Atmos. Chem. Phys., 13, 1853-
707 1877, https://doi.org/10.5194/acp-13-1853-2013, 2013.

National Emission Ceilings Directive (NEC) reporting status, doi:10.2800/984979, https://www.eea.europa.eu/themes/air/national-emission-ceilings/nec-directive-reporting-status-2018, 2018.

Nenes, A.; Pandis, S. N.; Pilinis, C.: ISORROPIA: A New Thermodynamic Equilibrium Model for Multiphase Multicomponent Inorganic Aerosols. Aquat. Geoch., 4, 123-152, 1998.

Nowak, J. B., Neuman, J. A., Bahreini, R., Middlebrook, A. M., Holloway, J. S., McKeen, S. A., Parrish, D. D., Ryerson, T. B., and Trainer, M.: Ammonia sources in the California South Coast Air Basin and their impact on ammonium nitrate formation, Geophys. Res. Lett., 39, L07804, https://doi.org/10.1029/2012GL051197, 2012.

Petetin, H., Sciare, J., Bressi, M., Gros, V., Rosso, A., Sanchez, O., Sarda-Estève, R., Petit, J.-E., and Beekmann, M.: Assessing the ammonium nitrate formation regime in the Paris megacity and its representation in the CHIMERE model, Atmos. Chem. Phys., 16, 10419-10440, https://doi.org/10.5194/acp-16-10419-2016, 2016.

Petit, J.-E., Favez, O., Sciare, J., Crenn, V., Sarda-Estève, R., Bonnaire, N., Močnik, G., Dupont, J.-C., Haeffelin, M., and Leoz-Garziandia, E.: Two years of near real-time chemical composition of submicron aerosols in the region of Paris using an Aerosol Chemical Speciation Monitor (ACSM) and a multi-wavelength Aethalometer, Atmos. Chem. Phys., 15, 2985-3005, https://doi.org/10.5194/acp-15-2985-2015, 2015.

Pinder, R. W., Adams, P. J., Pandis, S.N., and Gilliland, A. B.: Temporally resolved ammonia emission inventories: current estimates, evaluation tools, and measurement needs, J. Geophys. Res., 111, D16310, http://dx.doi.org/10.1029/2005JD006603, 2006.

Pope III, C. A., Ezzati M., and Dockery, D. W.: Fine-particulate air pollution and life expectancy in the United States, New England J. Med., 360 (4), 376-386, 2009.

Ramanantenasoa, M. M. J., Gilliot, J.-M., Mignolet, C., Bedos, C., Mathias, E., Eglin, T., Makowski, D., and Génermont, S.: A new framework to estimate spatio-temporal ammonia emissions due to nitrogen fertilization in France, Science of The Total Environment, 645, 205 – 219, https://doi.org/10.1016/j.scitotenv.2018.06.202, 2018.

Rockström, J., Steffen, W., Noone, K., Persson, A., Chapin Iii, F. S., Lambin, E. F., Lenton, T. M., Scheffer, M., Folke, C., Schellnhuber, H. J., Nykvist, B., de Wit, C. A., Hughes, T., van der Leeuw, S., Rodhe, H., Sörlin, S., Snyder, P. K., Costanza, R., Svedin, U., Falkenmark, M., Karlberg, L., Corell, R. W., Fabry, V. J., Hansen, J., Walker, B., Liverman, D., Richardson, K., Crutzen, P., and Foley, J. A.: Planetary boundaries: Exploring the safe operating space for humanity, Ecology and Society, 14, 2009.

741 Rodgers, C. D.: Inverse Methods for Atmospheric Sounding: Theory and Practice, vol. 2 of Series
742 on Atmospheric, Oceanic and Planetary Physics, edited by: Taylor, F. W., World Scientific, 2000.

743 Salmond, J. A., and McKendry, I. G.: A Review of Turbulence in the Very Stable Nocturnal
744 Boundary Layer and Its Implications for Air Quality, Progress in Physical Geography, 29 (2), 171–
745 188, 2005.

746 Schaap, M., Timmermans, R., Roemer, M., Boersen, G., Builtjes, P., Sauter, F., Velders, G., and
747 Beck, J.: The LOTOS-EUROS model: Description, validation and latest developments, Int. J.
748 Environ. Pollut., 32, 270–290, doi:10.1504/IJEP.2008.017106, 2008.

749 Shephard, M.W., and Cady-Pereira, K.E.: Cross-track Infrared Sounder (CrIS) satellite
750 observations of tropospheric ammonia, Atmos. Meas. Tech., 8, 1323-1336, 2015.

751 Shephard, M. W., Cady-Pereira, K. E., Luo, M., Henze, D. K., Pinder, R. W., Walker, J. T., Rinsland,
752 C. P., Bash, J. O., Zhu, L., Payne, V. H., and Clarisse, L.: TES ammonia retrieval strategy and global
753 observations of the spatial and seasonal variability of ammonia, Atmos. Chem. Phys., 11, 10743–
754 10763, doi:10.5194/acp-11-10743-2011, 2011.

755 Skjøth, C. A., Geels, C., Berge, H., Gyldenkærne, S., Fagerli, H., Ellermann, T., Frohn, L. M.,
756 Christensen, J., Hansen, K. M., Hansen, K., and Hertel, O.: Spatial and temporal variations in
757 ammonia emissions – a freely accessible model code for Europe, Atmos. Chem. Phys., 11, 5221-
758 5236, https://doi.org/10.5194/acp-11-5221-2011, 2011.

759 Skyllakou, K., Murphy, B. N., Megaritis, A. G., Fountoukis, C., and Pandis, S. N.: Contributions of
760 local and regional sources to fine PM in the megacity of Paris, Atmos. Chem. Phys., 14, 2343-
761 2352, https://doi.org/10.5194/acp-14-2343-2014, 2014.

762 Sutton, M. A., Bleeker, A., Howard, C., Bekunda, M., Grizzetti, B., de Vries, W., van Grinsven, H.,
763 Abrol, Y., Adhya, T., BillenG. and. Davidson, E., Datta, A., Diaz, R., Erisman, J., Liu, X., Oenema,
764 O., Palm, C., Raghuram, N., Reis, S., Scholz, R., Sims, T., Westhoek, H., Zhang, F., with
765 contributions from Ayyappan, S., Bouwman, A., Bustamante, M., Fowler, D., Galloway, J., Gavito,
766 M., Garnier, J., Greenwood, S., Hellums, D., Holland, M., Hoysall, C., Jaramillo, V., Klimont, Z.,
767 Ometto, J., Pathak, H., Plocq Fichelet, V., Powlson, D., Ramakrishna, K., Roy, A., Sanders, K.,
768 Sharma, C., Singh, B., Singh, U., Yan, X., and Zhang, Y.: Our Nutrient World: The challenge to
769 produce more food and energy with less pollution. Global Overview of Nutrient Management,
770 Centre for Ecology & Hydrology on behalf of the Global Partnership on Nutrient Management
771 and the International Nitrogen Initiative, 114 pp., 2013.

772 Stuhlmann, R., Rodriguez, A., Tjemkes, S., Grandell, J., Arriaga, A., Bézy, J.-L., Aminou, D., and
773 Bensi, P.: Plans for EUMETSAT's Third Generation Meteosat (MTG) Geostationary Satellite
774 Program, Adv. Space Res., 36, 975–981, 2005.

775 Toro, R.A., Canales, M., Flocchini, R.G., Morales, R.G.E., and Leiva G, M.A.: Urban atmospheric
776 ammonia in Santiago City, Chile, Aerosol Air Qual. Res., 14: 33–44, doi:
777 10.4209/aaqr.2012.07.0189, 2014.

778 Van Damme, M., Clarisse, L., Heald, C. L., Hurtmans, D., Ngadi, Y., Clerbaux, C., Dolman, A. J.,
779 Erisman, J. W., and Coheur, P. F.: Global distributions, time series and error characterization of
780 atmospheric ammonia (NH3) from IASI satellite observations, Atmos. Chem. Phys., 14, 2905–
781 2922, https://doi.org/10.5194/acp-14-2905-2014, 2014a.

782 Van Damme, M., Wichink Kruit, R. J., Schaap, M., Clarisse, L., Clerbaux, C., Coheur, P.-F.,
783 Dammers, E., Dolman, A. J., and Erisman, J. W.: Evaluating four years of atmospheric ammonia
784 (NH_3) over Europe using IASI satellite observations and LOTOS-EUROS model results, J. Geophys.
785 Res.-Atmos., 119, 9549-9566, 2014b.

786 Van Damme, M., Erisman, J. W., Clarisse, L., Dammers, E., Whitburn, S., Clerbaux, C., Dolman, A.
787 J., and Coheur, P.-F.: Worldwide spatiotemporal atmospheric ammonia (NH_3) columns variability
788 revealed by satellite, Geophys. Res. Lett., 42 (20), 8660-8668, 2015a.

789 Van Damme, M., Clarisse, L., Dammers, E., Liu, X., Nowak, J. B., Clerbaux, C., Flechard, C. R.,
790 Galy-Lacaux, C., Xu, W., Neuman, J. A., Tang, Y. S., Sutton, M. A., Erisman, J. W., and Coheur, P.
791 F.: Towards validation of ammonia (NH_3) measurements from the IASI satellite, Atmos. Meas.
792 Tech., 8, 1575-1591, https://doi.org/10.5194/amt-8-1575-2015, 2015b.

793 Van Damme, M., Whitburn, S., Clarisse, L., Clerbaux, C., Hurtmans, D., and Coheur, P.-F.: Version
794 2 of the IASI NH_3 neural network retrieval algorithm: near-real-time and reanalysed datasets,
795 Atmos. Meas. Tech., 10, 4905-4914, https://doi.org/10.5194/amt-10-4905-2017, 2017.

796 Van Damme, M., Clarisse, L., Whitburn, S., Hadji-Lazaro J., Hurtmans, D., Clerbaux, C., and
797 Coheur, P.-F.: Industrial and agricultural ammonia point sources exposed, Nature, 564 (7734):
798 99, DOI: 10.1038/s41586-018-0747-1, 2018.

799 van Vuuren, D. P., Edmonds, J., Kainuma, M. et al. he Representative Concentration Pathways:
800 An overview, Clim. Change, 109 (1–2), 5–31, https://doi.org/10.1007/s10584-011-0148-z, 2011.

801 Volten, H., Bergwerff, J. B., Haaima, M., Lolkema, D. E., Berkhout, A. J. C., van der Hoff, G. R.,
802 Potma, C. J. M., Wichink Kruit, R. J., van Pul, W. A. J., and Swart, D. P. J.: Two instruments based
803 on differential optical absorption spectroscopy (DOAS) to measure accurate ammonia
804 concentrations in the atmosphere, Atmos. Meas. Tech., 5, 413-427,
805 https://doi.org/10.5194/amt-5-413-2012, 2012.

806 Wang, S., Nan, J., Shi, C., Fu, Q., Gao, G., Wang, D., Cui, H., Saiz-Lopez A., and Zhou,B.:
807 Atmospheric ammonia and its impacts on regional air quality over the megacity of Shanghai,
808 China, Scientific Reports, 5, 15842, http://dx.doi.org/10.1038/srep15842, 2015.

809 Warner, J. X., Dickerson, R. R., Wei, Z., Strow, L. L., Wang, Y., and Liang, Q.: Increased
810 atmospheric ammonia over the world's major agricultural areas detected from space, Geophys.
811 Res. Lett., doi: 10.1002/2016gl072305, 2017.

812 Warner, J. X., Wei, Z., Strow, L. L., Dickerson, R. R., and Nowak, J. B.: The global tropospheric
813 ammonia distribution as seen in the 13-year AIRS measurement record, Atmos. Chem. Phys., 16,
814 5467-5479, https://doi.org/10.5194/acp-16-5467-2016, 2016.

815 Watson, J. G., Chow, J. C., Lurmann, F. W., and Musarra, S. P.: Ammonium Nitrate, Nitric Acid,
816 and Ammonia Equilibrium in Wintertime Phoenix, Arizona. Air & Waste, 44 (4), 405–412, 1994.

817 Whitburn, S., Van Damme, M., Clarisse, L., Bauduin, S., Heald, C., Hadji-Lazaro, J., Hurtmans, D.,
818 Zondlo, M., Clerbaux, C., and Coheur, P.-F.: A flexible and robust neural network IASI-NH3
819 retrieval algorithm, J. Geophys. Res. Atmos., 121, 6581–6599,
820 https://doi.org/10.1002/2016JD024828, 2016.

821 Wilks, Daniel S.: Statistical Methods in the Atmospheric Sciences, 3rd ed. Oxford, Waltham, MA:
822 Academic Press, 2011.

823 Ye, X., Ma, Z., Zhang, J., Du, H., Chen, J., Chen, H., Yang, X., Gao, W. and Geng, F.: Important role
824 of ammonia on haze formation in Shanghai, Environ. Res. Lett., 6: 024019, doi:10.1088/1748-
825 9326/6/2/024019, 2011.

826 Zavyalov, V., Esplin, M., Scott, D., Esplin, B., Bingham, G., Hoffman, E., Lietzke, C., Predina, J.,
827 Frain, R., Suwinski, L., Han, Y., Major, C., Graham, B., and Phillips, L.: Noise performance of the
828 CrIS instrument, J. Geophys. Res., doi: 10.1002/2013JD020457, 2013.

829 Zhang, Q. J., Beekmann, M., Drewnick, F., Freutel, F., Schneider, J., Crippa, M., Prevot, A. S. H.,
830 Baltensperger, U., Poulain, L., Wiedensohler, A., Sciare, J., Gros, V., Borbon, A., Colomb, A.,
831 Michoud, V., Doussin, J.-F., Denier van der Gon, H. A. C., Haeffelin, M., Dupont, J.-C., Siour, G.,
832 Petetin, H., Bessagnet, B., Pandis, S. N., Hodzic, A., Sanchez, O., Honoré, C., and Perrussel, O.:
833 Formation of organic aerosol in the Paris region during the MEGAPOLI summer campaign:
834 evaluation of the volatility-basis-set approach within the CHIMERE model, Atmos. Chem. Phys.,
835 13, 5767-5790, https://doi.org/10.5194/acp-13-5767-2013, 2013.

836 Zhao, M., Wang, S., Tan, J., Hua, Y., Wu, D., and Hao, J.: Variation of urban atmospheric
837 ammonia pollution and its relation with PM2.5 chemical property in winter of Beijing, China,
838 Aerosol Air Qual. Res., 16, 1378–1389, https://doi.org/10.4209/aaqr.2015.12.0699, 2016.

839 Zhu, L., Henze, D. K., Cady-Pereira, K. E., Shephard, M. W., Luo, M., Pinder, R. W., Bash, J. O., and
840 Jeong, G.: Constraining U.S. ammonia emissions using TES remote sensing observations and the
841 GEOS-Chem adjoint model, J. Geophys. Res.-Atmos., 118, 3355–3368, doi:10.1002/jgrd.50166,
842 2013.

Atmos. Chem. Phys. Discuss., https://doi.org/10.5194/acp-2019-138
Manuscript under review for journal Atmos. Chem. Phys.
Discussion started: 25 March 2019

Atmospheric Chemistry and Physics Discussions

FIGURES

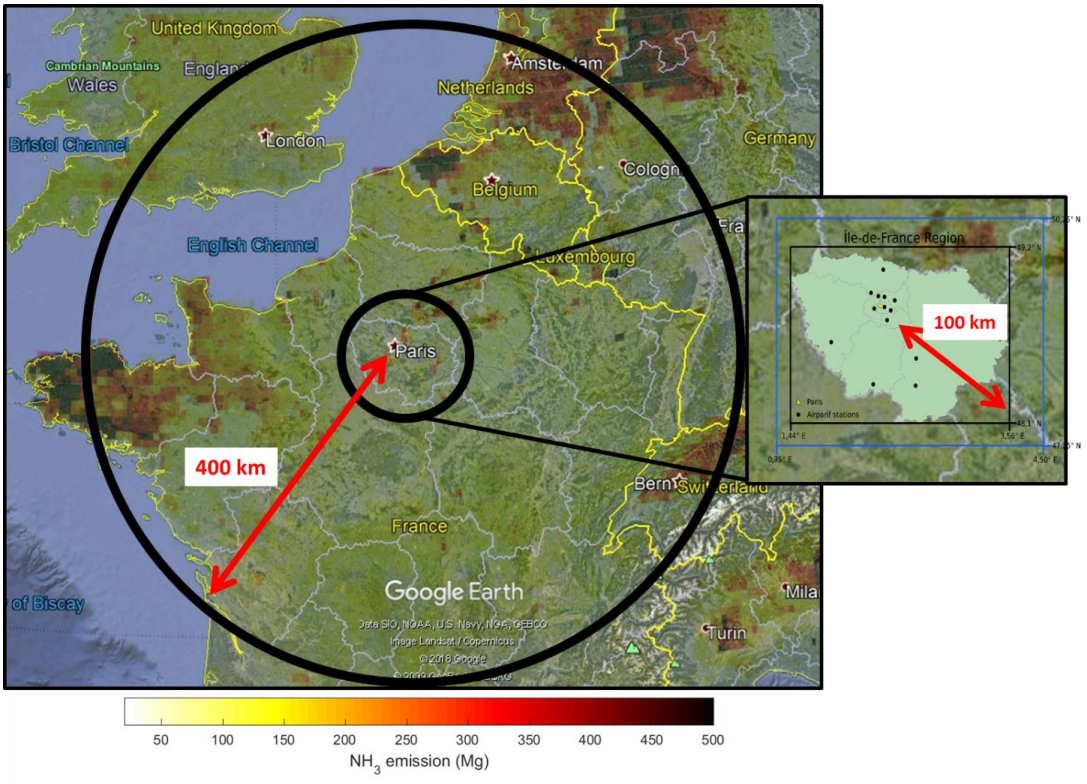

Figure 1: Region of analysis: 400 km radius-circle around the Paris megacity and 100 km around Paris. The latter is representative of the Ile-de-France (IdF) region where the Airparif PM observational network is located. Black points are the locations of the Airparif stations measuring hourly $PM_{2.5}$ concentration at the surface. The black (blue) box delimitates the IdF region in which the IASI NH_3 (ECMWF) data have been considered. The overlay represents NH_3 emissions (in Mg per year and per cell of 0.1°x0.1°) derived from the EMEP inventory for 2015.

Atmos. Chem. Phys. Discuss., https://doi.org/10.5194/acp-2019-138
Manuscript under review for journal Atmos. Chem. Phys.
Discussion started: 25 March 2019

Atmospheric Chemistry and Physics Discussions

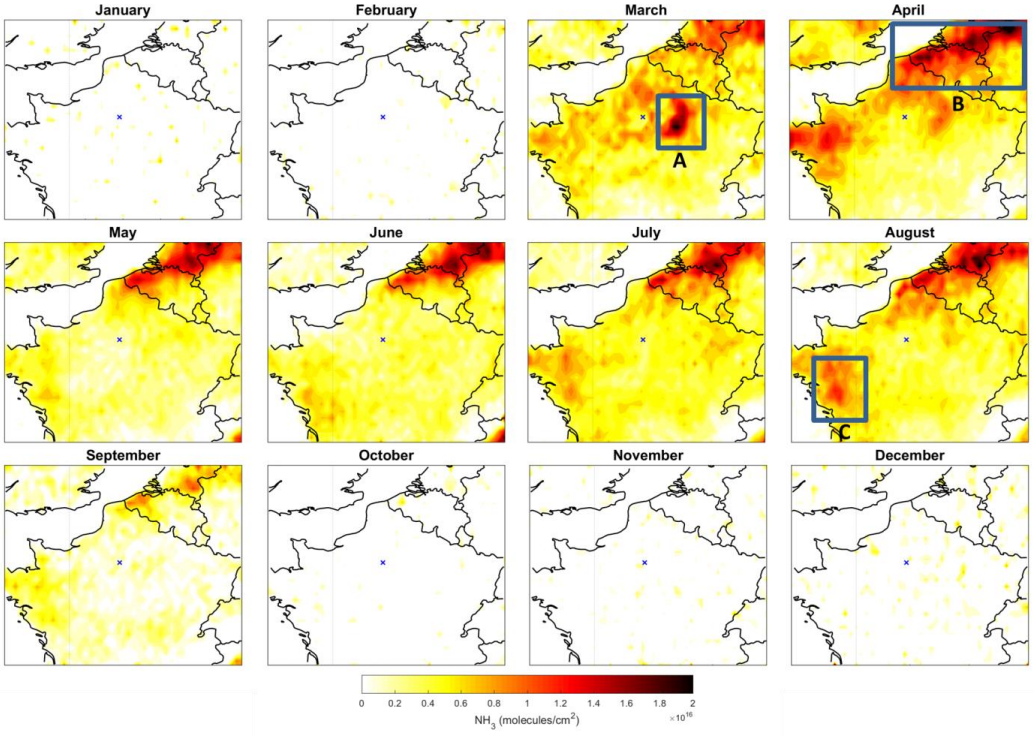

851

852 Figure 2: Monthly means of NH_3 total columns (molecules/cm²) derived from 10 years (2008-
853 2017) of IASI NH_3-retrieved columns. The blue cross indicates Paris location.

854

Atmos. Chem. Phys. Discuss., https://doi.org/10.5194/acp-2019-138
Manuscript under review for journal Atmos. Chem. Phys.
Discussion started: 25 March 2019

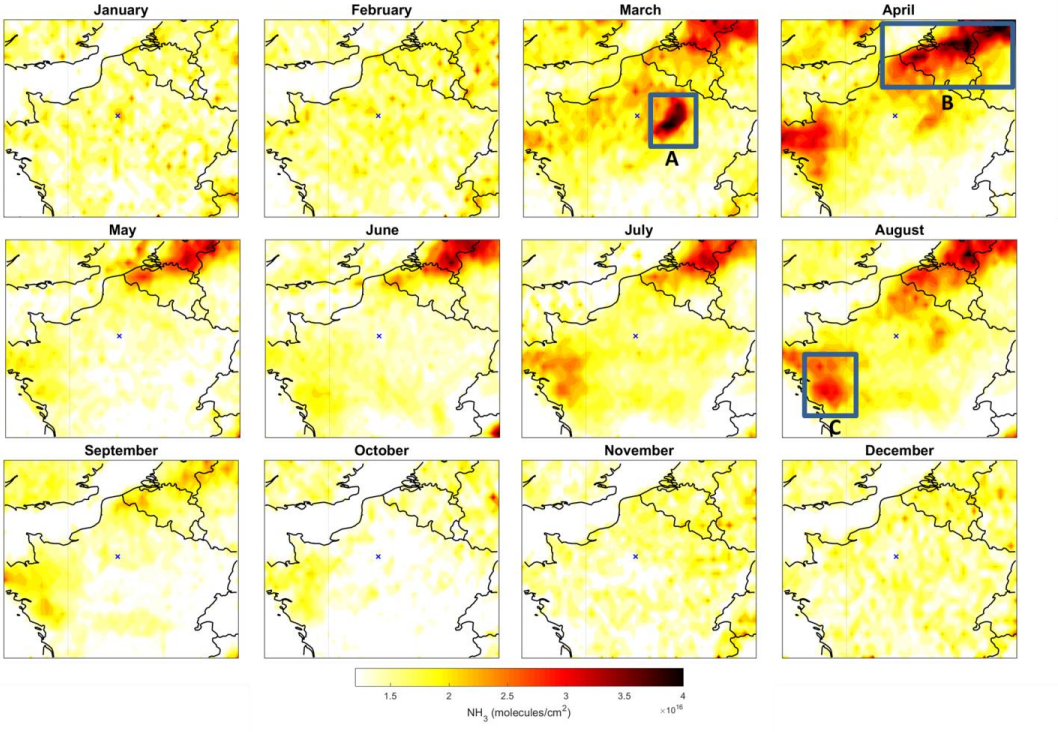

855

856 Figure 3: Monthly means of NH_3 total columns (molecules/cm²) derived from 5 years (2013-
857 2017) of CrIS NH_3-retrieved columns. The blue cross indicates Paris location.

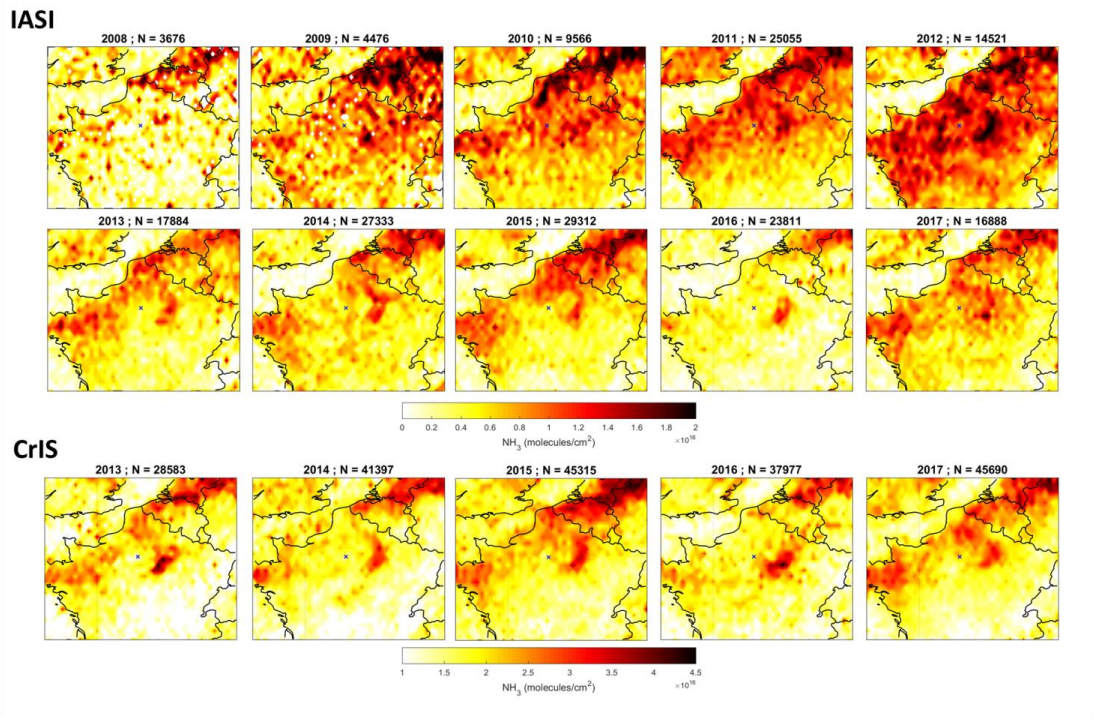

858

859 Figure 4: Maps of monthly mean NH_3 total columns (molecules/cm²) in March-April period
860 derived from IASI from 2008 to 2017 and CrIS from 2013 to 2017.

Atmos. Chem. Phys. Discuss., https://doi.org/10.5194/acp-2019-138
Manuscript under review for journal Atmos. Chem. Phys.
Discussion started: 25 March 2019

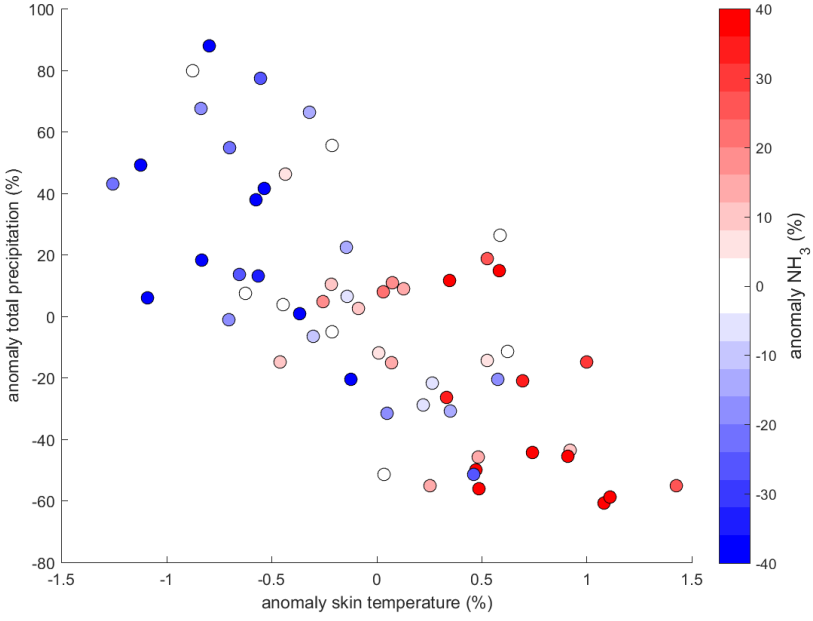

Figure 5: Scatter plot of monthly mean anomaly (relative to the 10-years – 2008 to 2017 - monthly average) of total precipitation versus skin temperature derived from ECMWF from March to August in the domain, and color coded by the NH_3 total columns anomaly derived from IASI.

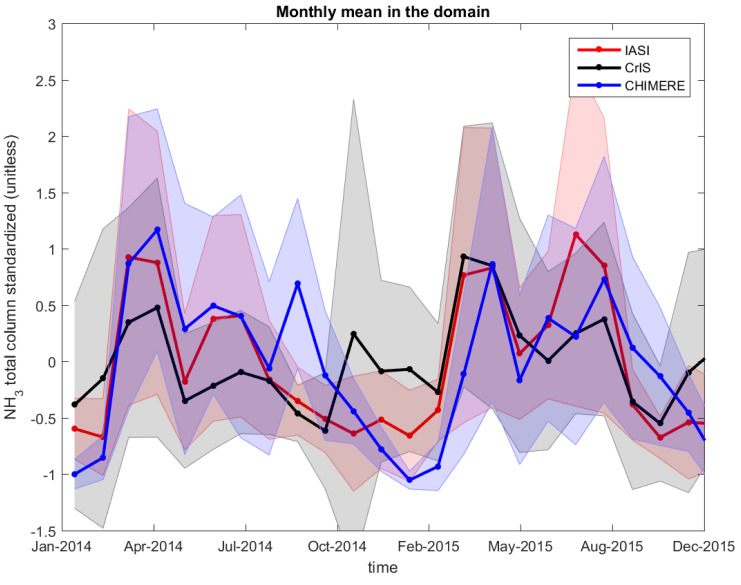

866

867 Figure 6: Standardized monthly mean concentrations derived from IASI (red), CrIS (black) and
868 CHIMERE (blue) for 2014 and 2015. Shaded areas correspond to the one-sigma standard
869 deviation around the means.

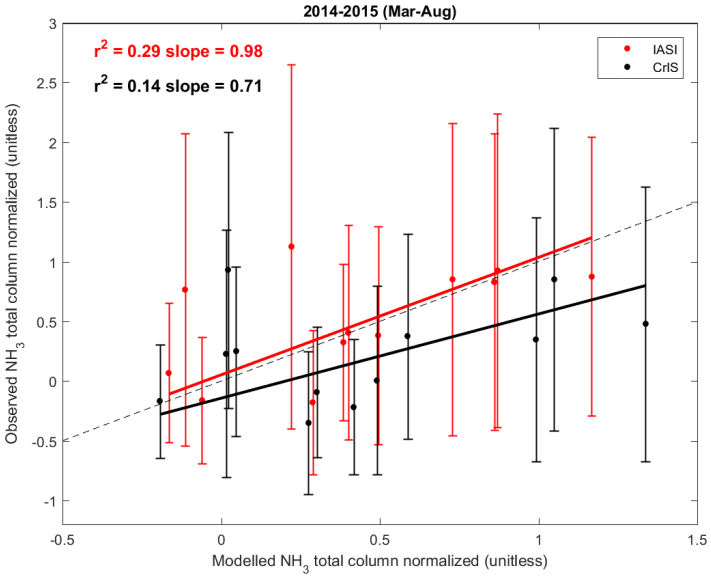

870

871 Figure 7: Correlation plots between monthly means NH_3 standardized concentrations derived
872 from satellite observations (IASI in red and CrIS in black) and the CHIMERE outputs for the
873 March to August months of 2014 and 2015. The 1:1 line is represented in the dashed line.

Atmos. Chem. Phys. Discuss., https://doi.org/10.5194/acp-2019-138
Manuscript under review for journal Atmos. Chem. Phys.
Discussion started: 25 March 2019

Atmospheric Chemistry and Physics Discussions

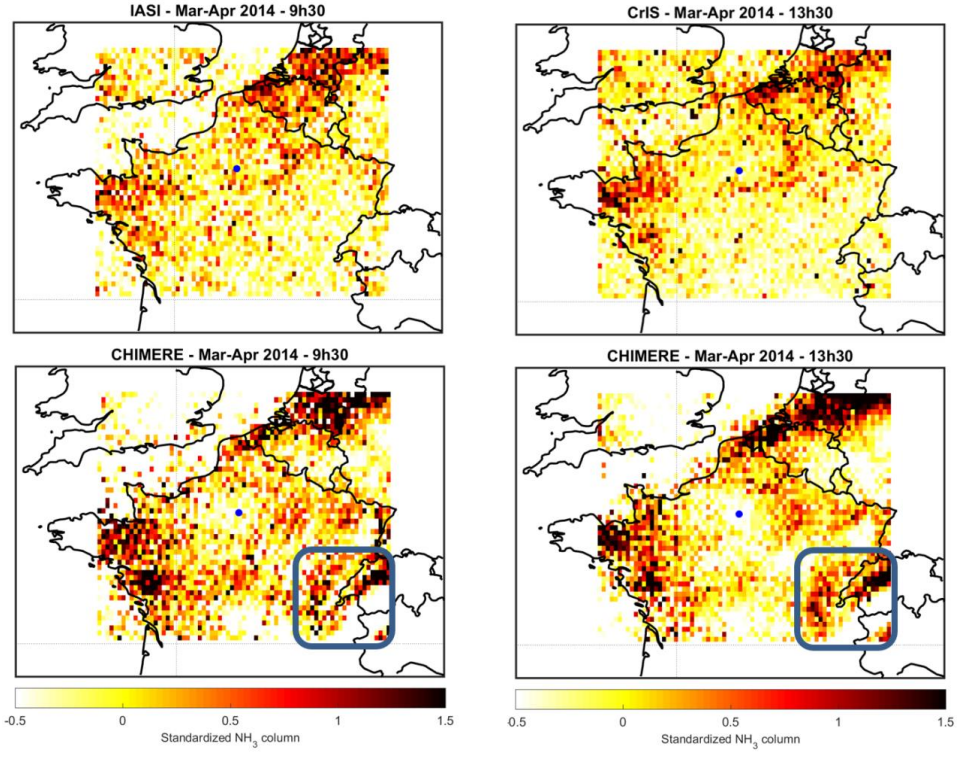

874

875 Figure 8: Standardized NH_3 column derived from the satellite instruments (IASI = top left panel,
876 and CrIS = top right panel) and the corresponding NH_3 column derived from the CHIMERE model
877 (coincident with IASI – bottom left panel, and coincident with CrIS – bottom left panel) for
878 March-April 2014. Blue dots indicate Paris location.

Atmos. Chem. Phys. Discuss., https://doi.org/10.5194/acp-2019-138
Manuscript under review for journal Atmos. Chem. Phys.
Discussion started: 25 March 2019

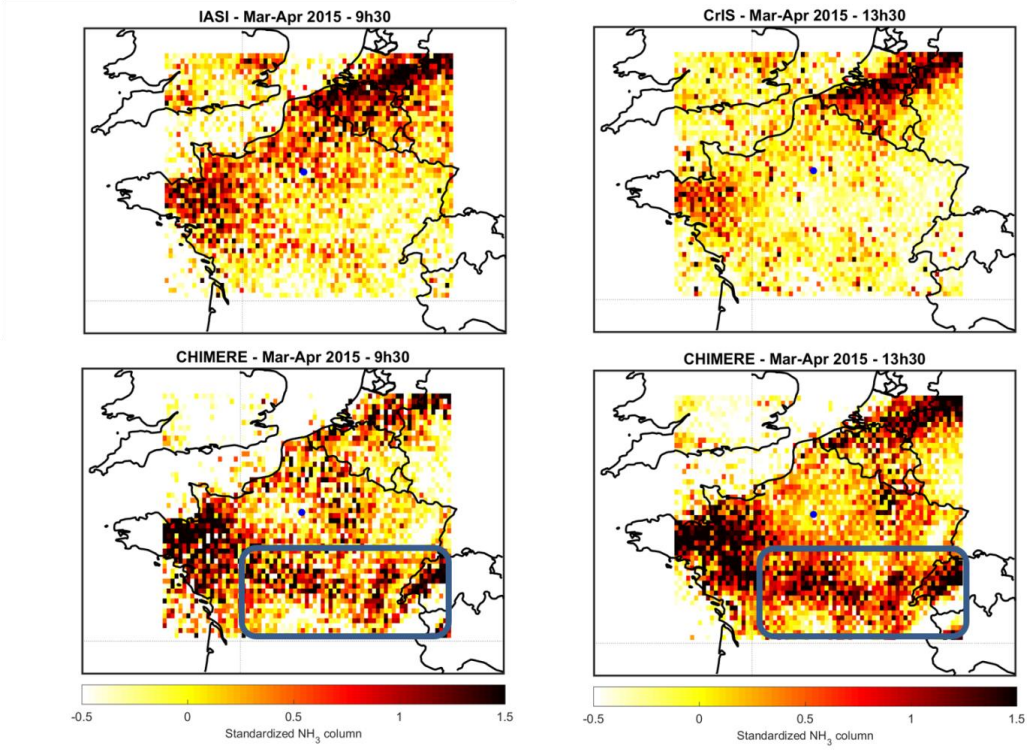

879

880 Figure 9: Same than Figure 7 but for March-April 2015.

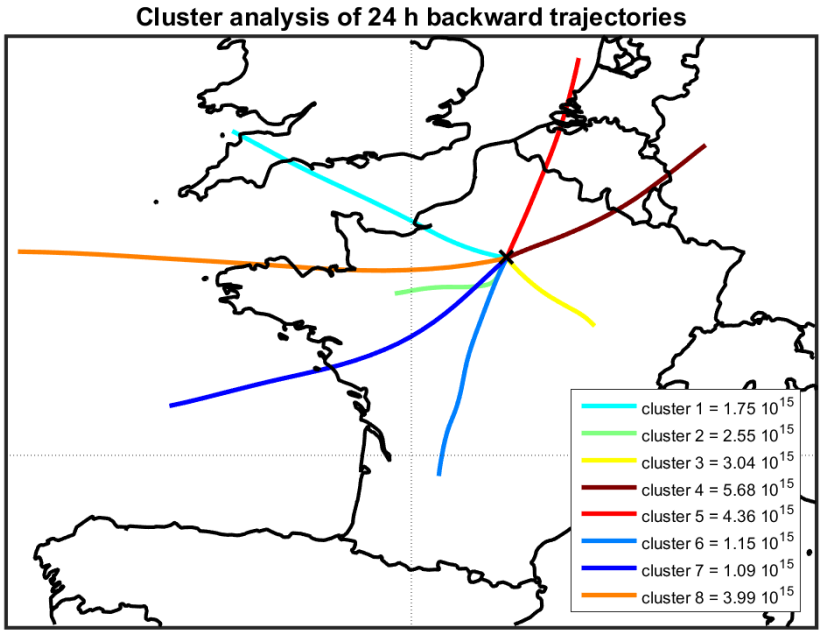

Figure 10: Cluster analysis of 24-h backward trajectories arriving in spring in Paris (from February 15th to May 15th for the 2013-2016 period) using HYSPLIT-4 model obtained from the NOAA Air Resources Laboratory. Mean trajectories of the 8 clusters are shown in different colors, associated with the NH_3 concentrations measured by IASI in the IdF region (in molecules/cm^{-2}).

Atmos. Chem. Phys. Discuss., https://doi.org/10.5194/acp-2019-138
Manuscript under review for journal Atmos. Chem. Phys.
Discussion started: 25 March 2019

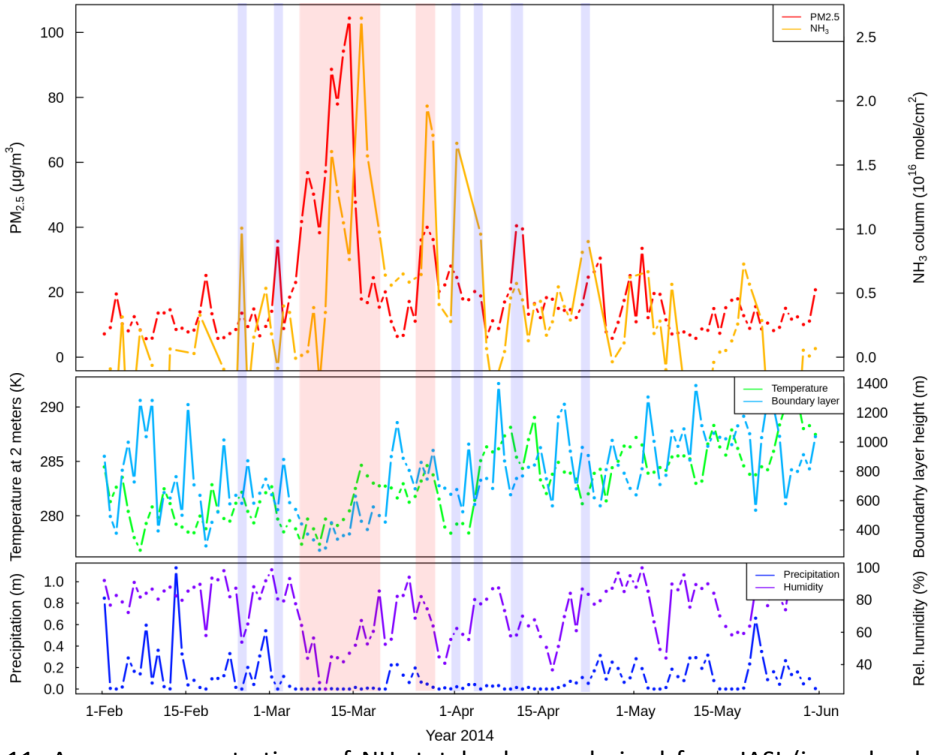

Figure 11: Average concentrations of NH_3 total columns derived from IASI (in molecules/cm²; orange, upper panel) and $PM_{2.5}$ derived from the Airparif network selected within 2 hours from the IASI overpass (in µg/m³; red, upper panel) for 2014 as example. Periods of simultaneous (independent) enhancements of NH_3 and PM concentrations are represented with red (blue) areas, i.e. case A (case B). Temperature at 2 meters (in Kelvin; green, middle panel), boundary layer height (in meter; blue, middle panel), precipitation (in meter; dark blue, lower panel), and relative humidity (in percent; purple, lower panel) derived from the ECMWF ERA-interim.

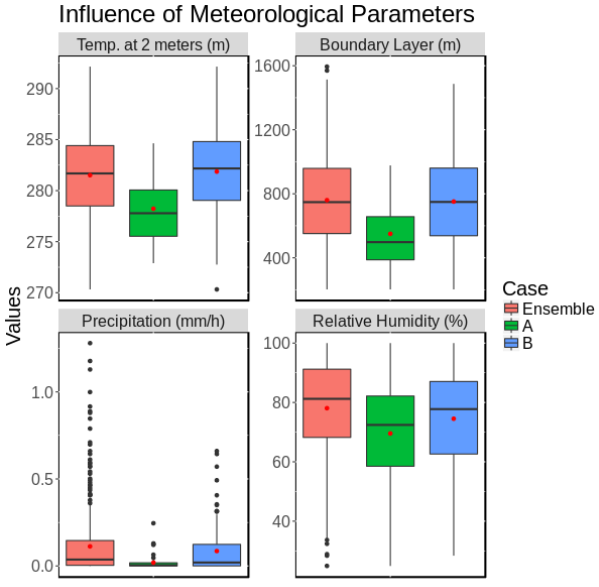

Figure 12: Statistical distributions of meteorological parameters corresponding to case A, case B, and all observations derived from 2013 to 2016. The medians and the quartiles are presented by center lines and borders of the boxes, respectively. The mean values are indicated by red points, and the extreme values (i.e. those beyond Q1 - 1.5 IQR and Q3 + 1.5 IQR) by black points.

Atmos. Chem. Phys. Discuss., https://doi.org/10.5194/acp-2019-138
Manuscript under review for journal Atmos. Chem. Phys.
Discussion started: 25 March 2019

Atmospheric Chemistry and Physics Discussions

900 **TABLE**

	Satellite	Overpass time (LT)	Time coverage	Nadir spatial resolution (km)	Spectral range (cm^{-1})	Spectral resolution (cm^{-1})	Spectral Noise* (K) @270K @ 970 cm^{-1}	References
IASI	Metop-A/B	9.30 (AM/PM)	2006-present	12	645–2760	0.5 (apodized)	~0.2	Clerbaux et al., 2009
CrIS	Suomi-NPP	1.30 (AM/PM)	2011-present	14	645–1095; 1210–1750; 2155–2550	0.625; (unapodized)	~0.05	Zavyalov et al., 2013

*Spectral noise comparison values in main ammonia spectral region (~970 cm^{-1}) obtained from Zavyalov et al., 2013.

901 Table 1: Instrumental specifications for the IASI and CrIS satellite instruments.